Green Chemistry

PAPER

View Article Online
View Journal | View Issue

Cite this: *Green Chem.*, 2024, **26**, 4032

Employing photocurable biopolymers to engineer photosynthetic 3D-printed living materials for production of chemicals†

Gábor Szilveszter Tóth,[a] Oskar Backman,[b] Tiia Siivola,[a] Wenyang Xu,[b] Sergey Kosourov,[a] Vilja Siitonen,[a] Chunlin Xu[b] and Yagut Allahverdiyeva *[a]

Photosynthetic microorganisms, such as cyanobacteria and microalgae, have great potential as living cell factories for chemical and fuel production. Immobilisation of cells is an effective technique for enhancing productivity and longevity of the production system, as well as aiding in the separation of cells from the medium. Alginate crosslinked with divalent ions is commonly used for immobilisation, however its ionic crosslinking is reversible in high ionic strength or in the presence of chelating agents leading to matrix degradation. To address these challenges, photocurable materials present a potential solution, especially when coupled with 3D-printing technologies to create complex, tunable 3D architectures for various applications. In this context, we propose a bioink composed of alginate, photocurable galactoglucomannan-methacrylate and photosynthetic cells for 3D-printing green biocatalysts for solar-chemical production. We demonstrate the applicability of this photocurable bioink for the immobilisation of photosynthetic microbes either capable of producing ethylene (specifically-engineered *Synechocystis* cell factories) or transforming cyclohexanone to ε-caprolactone (specifically-engineered *Chlamydomonas* cell factories), both of which are industrially relevant chemicals. Films produced from photocurable bioinks demonstrate high mechanical stress tolerance compared to films prepared *via* conventional ionic crosslinking, showing resistance to high ionic strength in the medium. Furthermore, both *Synechocystis* and *Chlamydomonas* cells entrapped within 200 μm-thick hydrogel layers, 3D-printed on glass support surfaces, demonstrated notably high (ethylene) or similar (biotransformation of cyclohexanone to ε-caprolactone) production titres and space–time yields compared to the conventional biocatalysts. These engineered living materials, being biocompatible and biobased, particularly when used in conjunction with 3D-printing, provide convenient scalability and potential to enhance sustainability in the chemical industry.

Received 3rd November 2023,
Accepted 23rd February 2024

DOI: 10.1039/d3gc04264b

rsc.li/greenchem

1. Introduction

Photosynthetic microbes, such as cyanobacteria and green algae, utilise solar energy to oxidise water and fix CO_2. The electrons and organic carbon gained this way are in turn used to generate biomass, as well as to synthesize specific target chemicals. With low nutrient requirements, high metabolic diversity and short doubling time, microalgae and cyanobacteria are suitable chassis for engineering living cell factories for the sustainable production of various solar chemicals, ranging from biofuels and bulk materials to high-value products.[1–3]

Solid-state photosynthetic cell factories offer several distinct advantages over conventional suspension cultures.[4,5] In these systems, photosynthetic microbes are enclosed within polymer matrices, restricting cell division and promoting a shift towards biocatalytic production rather than biomass accumulation. Furthermore, the longevity of the cells is significantly increased within the matrix, allowing for prolonged and continuous chemical production. Additionally, entrapment simplifies the process of separating the cells from the medium and facilitates downstream processing of the products.[6,7] A wide variety of biopolymers can be utilised for the entrapment of microbes, offering different chemical and mechanical properties and high biocompatibility. Alginate (Alg), agarose, TEMPO-oxidised cellulose nanofibrils (TCNF) and nanocrystals (TCNC), as well as gelatine and carrageenan, represent a few examples of possible entrapment matrices. These biopolymers can be moulded into diverse architectures, such as beads, thin films or complex three-dimensional structures.[8–13] Thin artifi-

[a]*Molecular Plant Biology, Department of Life Technologies, University of Turku, 20014 Turku, Finland. E-mail: allahve@utu.fi*
[b]*Laboratory of Natural Materials Technology, Faculty of Science and Engineering, Åbo Akademi University, 20500 Turku, Finland*

† Electronic supplementary information (ESI) available. See DOI: https://doi.org/10.1039/d3gc04264b

cial films are particularly appealing for photosynthetic organisms, as they reduce the self-shading of cells, thereby enhancing light utilisation and production efficiency.[7] Among the most frequently used materials for thin-layer immobilisation is Alg crosslinked by Ca^{2+} or Ba^{2+}. However, this method comes with notable limitations.

For instance, the mechanical strength of Alg films may not be adequate for harsh production conditions. In scenarios where strong agitation is necessary, these films can break, compromising the stability of the setup. Additionally, the ionic crosslinking in Alg films is reversible, which leads to the degradation in environments with high ionic strength or in the presence of chelating agents.[10,14–16]

An approach to strengthen crosslinking involves the use of multiple polymers coupled with ionic interactions. Polyvinyl alcohol (PVA) and Ca^{2+} ions have demonstrated effectiveness in creating mechanically stable films. PVA not only provides stronger linkage by hydrogen bonds but also complements the ionic crosslinking. However, this method requires the films to be dried, which imposes additional stress on the cells. Although partial drying of the films under controlled humidity can help to address this issue,[10,17] uneven drying remains a challenge and can result in film heterogeneities. A promising method for creating homogenous films with reduced cell stress involves osmotic dehydration. This method allows for control over pore size and water content in the films.[18] However, the dehydration step is time-consuming, and regulating the thickness of the resulting films can be challenging.

To effectively tackle these challenges, the implementation of 3D-printing using a novel bioink composed of photocurable materials, Alg and photosynthetic microbes, presents a promising solution. Such an approach offers several advantages, including enhanced mechanical stability and the ability to introduce hierarchical structures, such as channels that simplify water and gas exchanges and improve mass transfer.

Photocuring is a technique used to covalently link polymer chains by harnessing light energy. Typically, functional groups like acrylates or methacrylates are polymerised in the presence of a photoinitiator. It is important to note that some photoinitiators have adverse effects on living cells[19] due to the production of free radicals that can harm cells and severely damage the photosynthetic machinery.[20] Currently, photocuring of biopolymers finds applications in medical science, where it is used to create hydrogel networks for reconstructive and plastic surgeries, dental materials, medical devices and support matrices for mammalian cell cultures.[19,21,22]

Different cell types require different geometries and matrix properties for optimal growth and morphology, and 3D-printing technologies allow for tailored structures to meet these requirements.[23–25] By coupling photosynthetic microbes with the 3D-printing of photocurable biopolymers, there is significant potential to create complex 3D architectures with enhanced mechanical stability, mimicking the structure of plant leaves. Such artificial leaves have been proposed for applications in chemical production platforms and atmospheric CO_2 capture.[26]

One readily available matrix material for 3D-printing and photocuring is galactoglucomannan-methacrylate (GGMMA). GGMMA is a hemicellulose derivative, a non-toxic, biocompatible and biodegradable material. Hemicellulose is the second most abundant polysaccharide in nature, right after cellulose. It can be obtained from by-products of the forest industry and agriculture. GGMMA is effective as a photo-crosslinker, adding mechanical tunability to nanocellulose-based 3D-printing inks, offering high printing fidelity. These inks have demonstrated their capability to support the growth of human pancreatic tumour cells and fibroblasts.[25]

Here, we demonstrate the utilisation of a composite ink comprising Alg, GGMMA and the photoinitiator, lithium phenyl-2,4,6-trimethylbenzoylphosphinate (LAP) for thin-layer immobilisation of photosynthetic microbes. The performance of thin Alg + GGMMA + LAP films, which were fabricated *via* 3D-printing and photocuring, was checked in two different production systems. In the first, we employed the engineered prokaryotic cyanobacterium *Synechocystis* sp. PCC 6803 possessing the heterologously-expressed Efe enzyme (hereafter referred to as *Synechocystis*). This engineered cyanobacterium is capable of producing ethylene from atmospheric CO_2 using light energy.[16,27] Ethylene is a vital building block for various commercially important polymers, which holds significant potential in green chemistry manufacturing.[28,29] In the second production system, we employed an engineered eukaryotic green alga, *Chlamydomonas reinhardtii* UVM11-CW/CHMO_PSAD clone 10 (hereafter referred to as *Chlamydomonas*), which was constructed to express a heterologous Baeyer–Villiger monooxygenase (BVMO), cyclohexanone monooxygenase (CHMO) capable of performing the biotransformation of cyclohexanone to ε-caprolactone. ε-caprolactone is another compound utilised by the polymer industry for the synthesis of different plastic products.[30]

We showed that the proposed composite material comprising Alg, GGMMA and LAP is compatible with photosynthetic cells, is suitable for 3D-printing of mechanically stable matrices including thin biofilms and does not hinder the production of target chemicals.

2. Results and discussion

2.1. 3D-printing of living materials using a nature-based photocurable bioink

The cells of the unicellular model cyanobacterium, *Synechocystis* or the unicellular model green alga *Chlamydomonas* were incorporated into the Alg + GGMMA + LAP formulation, which was then 3D-printed onto glass slides pre-treated with 3-(trimethoxysilyl)propyl methacrylate (TMPSM). The application of TMPSM facilitates better attachment of the ink to the substrate *via* covalent bonds. Subsequently, the 3D-printed films were photocured with 405 nm light for 10 minutes (Fig. 1, see the 'Experimental' section for further details). As a result, elastic biofilms with entrapped photosynthetic cells were firmly attached to the

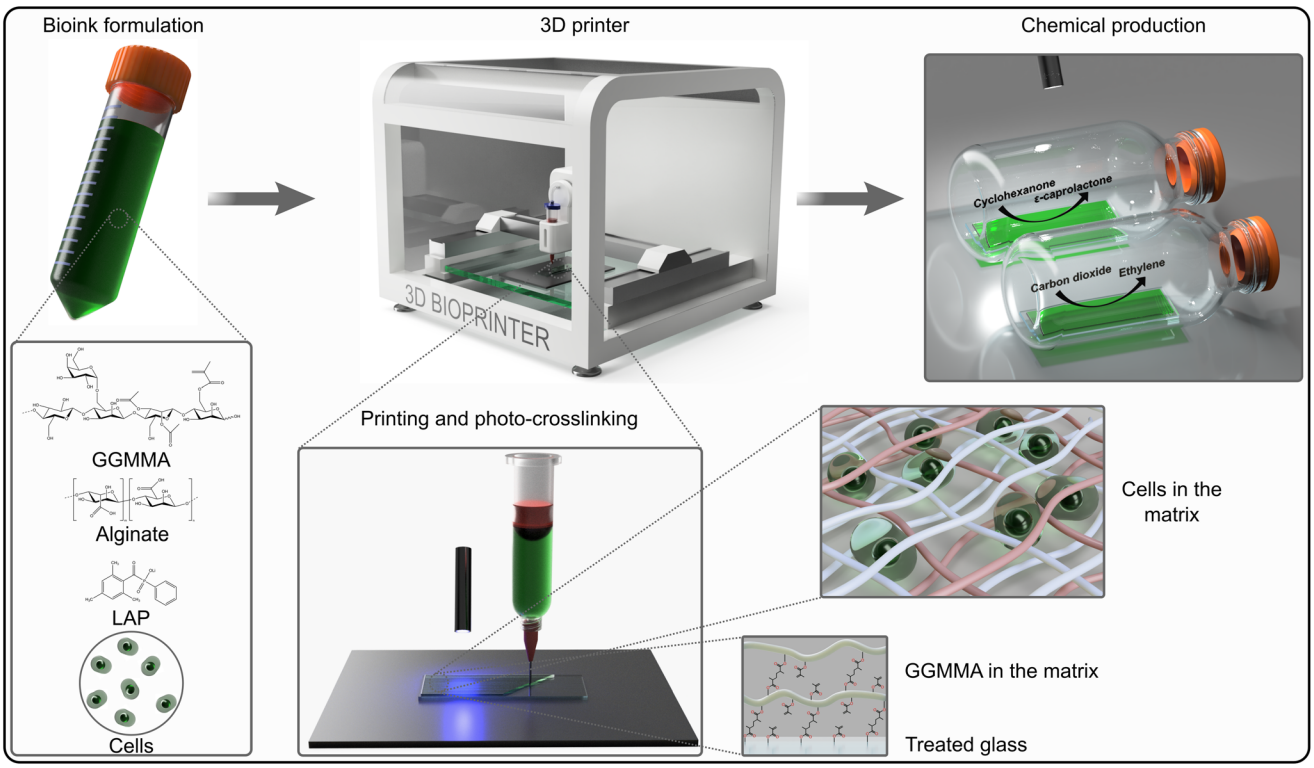

Fig. 1 Schematic representation of the 3D-printing of photosynthetic cells in photocurable ink for biocatalytic solar chemical production. The cells were mixed with Alg, GGMMA and LAP with final concentrations of 3% (w/v), 4% (w/v) and 0.05% (w/v) respectively then printed on a pre-treated glass surface using Brinter ONE multitool 3D bioprinter (Brinter, Finland). Crosslinking between GGMMA strands and attachment to the glass surface happened upon exposure to 405 nm light. The crosslinked films were used for photosynthetic production of ethylene and ε-caprolactone.

surface of the glass support, which provided additional mechanical stability.

During entrapment, the cells may experience several stress factors, including (i) shear stress during extrusion printing, (ii) exposure to high-intensity light during photocuring, and (iii) the presence of free radicals created by the photoinitiator upon light exposure. Both high-intensity light and free radicals can be damaging factors affecting the photosynthetic machinery.[31–33] Preliminary tests were conducted to assess the effects of different photoinitiator concentrations on cell fitness. They showed that 0.05% (w/v) LAP is effective for photocuring, while not being detrimental to cell growth (see ESI†). Therefore, this LAP concentration was applied in all the following formulations. To evaluate the cell fitness post-printing, photosynthetic activity, specifically photosystem II yield (Y(II)) of the entrapped cells, was monitored for 6 days. Immediately after entrapment, Y(II) was low in both *Synechocystis* (Fig. 2A) and *Chlamydomonas* cells (0.2 and 0.4, respectively) (Fig. 2B). This indicates decreased photosynthetic activity as a result of the accompanying stress. To recover the fitness of the entrapped cells, films were incubated either overnight for *Synechocystis* or 72 h for *Chlamydomonas* under low light (25 μmol photons m^{-2} s^{-1}), without agitation. Following the incubation, the Y(II) of both cyanobacteria and green algae increased to 0.5 and 0.7, respectively, reaching values typically observed during the growth phase (Fig. 2A and B). The Y(II) remained relatively stable throughout 3 days with a slight tendency to decline by the end of monitoring.

The results thus demonstrated that the Alg + GGMMA + LAP matrix is a suitable formulation for the entrapment of *Synechocystis* and *Chlamydomonas* cells, without adversely affecting their photosynthetic activity. The initial decrease in Y(II) can be attributed to the stress induced during printing and the stress caused by the unintentional drying of the films during photocuring.[10,33,34] However, this transient decrease does not impede the long-term cell fitness.

2.2. Photo-rheology measurements to investigate mechanical and rheological properties of the Alg + GGMMA + LAP films

Photo-rheology measurements were conducted to investigate the photocuring kinetics of the Alg + GGMMA + LAP composite ink (3% (w/v) Alg, 4% (w/v) GGMMA and 0.05% (w/v) LAP) upon exposure to 405 nm light. The effect of cell entrapment on the curing process was investigated by introducing either *Synechocystis* or *Chlamydomonas* cells into the ink. After 20 s of light exposure, a sudden increase in the storage modulus (G') and the loss modulus (G'') was observed, indicating that gel formation of the composite ink took place (Fig. 3). The gel point, where G' exceeds G'', signifying the transition from fluid-like behaviour to elastic gel behaviour, was reached after ~30 s.[35]

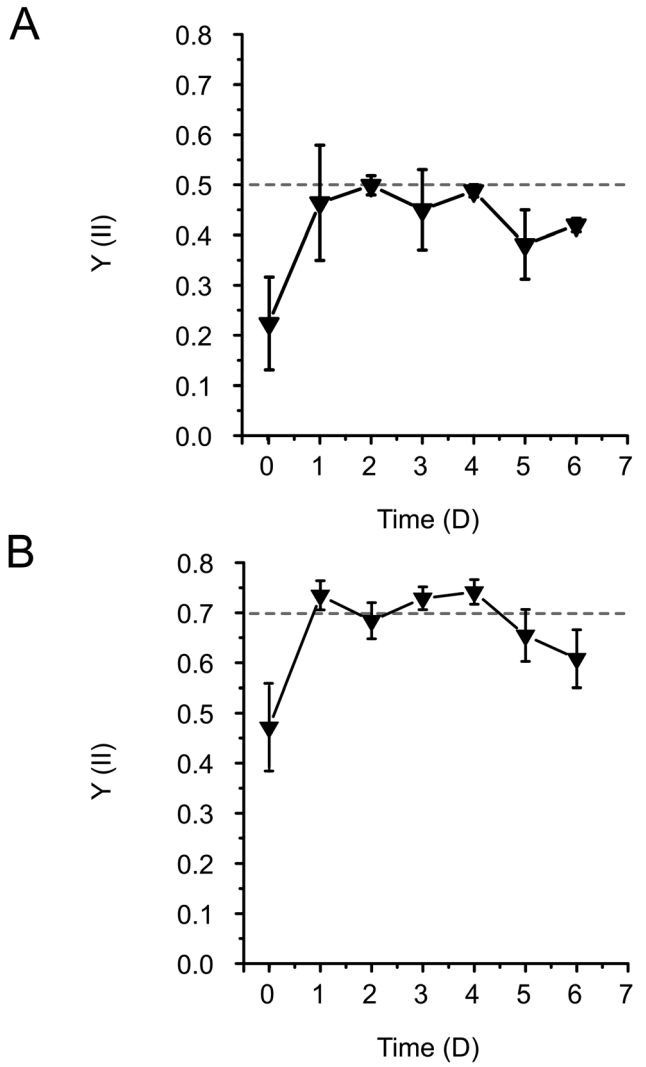

Fig. 2 The change of effective PSII yield (*Y*(II)) of immobilised cells during the 6-day adaptation period after 3D-printing and photocuring. *Y*(II) in (A) *Synechocystis* and (B) *Chlamydomonas* cells entrapped in 3D-printed films were measured by PAM 2000 fluorometer. The standard deviations are presented for 3 biological replicates containing 1–3 technical repetitions. The dashed line represents the *Y*(II) values observed during the growth phase.

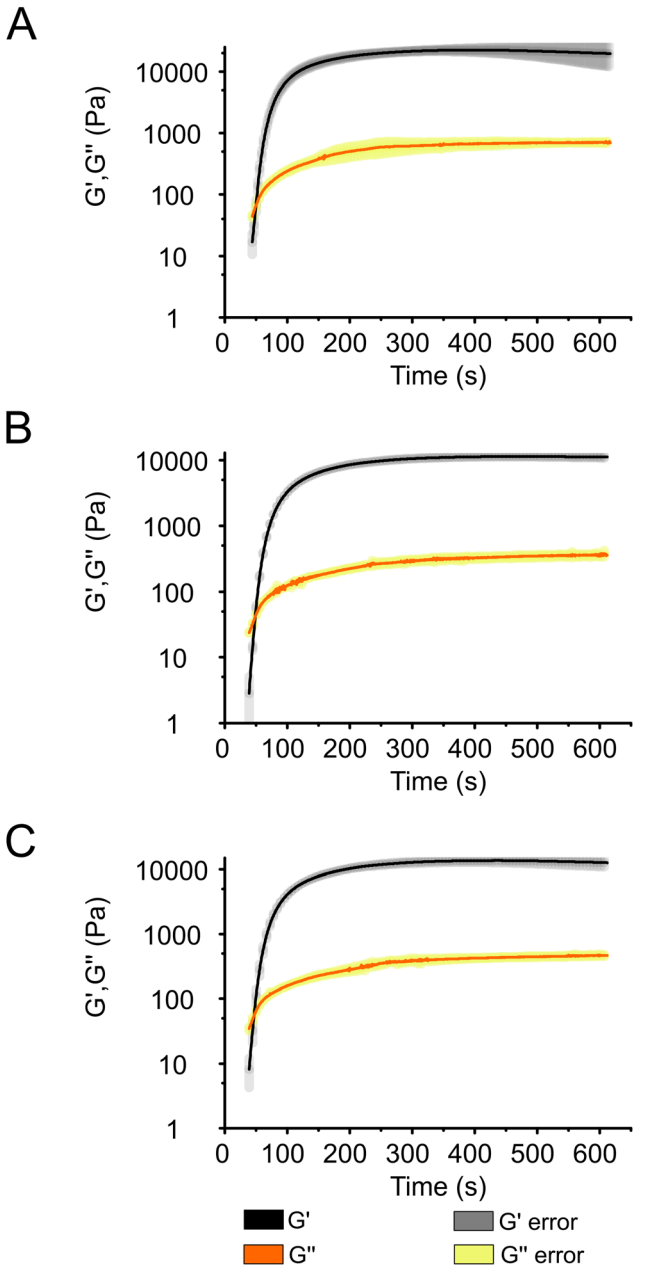

Fig. 3 Photo-rheology measurements describing the photocuring process of Alg + GGMMA + LAP ink. (A) Cell-free ink and inks loaded with (B) *Synechocystis* and (C) *Chlamydomonas* cells. Changes of storage modulus (*G*′) and loss modulus (*G*″) are shown after 20 s exposure to 405 nm light. Shading represents standard deviations.

The curing process neared completion after ~150 s in all samples (Fig. 3) as demonstrated by the curves reaching a plateau at this time point (Fig. 3), although, *G*′ continued to slightly increase throughout the 600 s measurement. As evident from Fig. 3, there was no difference in the curing dynamics between the cell-free ink (Fig. 3A) and the bioink loaded with *Synechocystis* or *Chlamydomonas* cells (Fig. 3B and C, respectively). However, there was a difference in the final value of *G*′, which was ~20 kPa in the cell-free ink and ~10 kPa in the cell-containing ink. These values are considerably higher than those obtained during the curing process of another photocurable ink composed of modified Alg and gelatine (300.4 Pa)[36] and comparable to photocurable formulations of TCNF and GGMMA (10–60 kPa).[25] As shown in Fig. 3, the curing progresses at the same pace in all samples. This indicates that the introduction of cells does not slow down the process by, *e.g.*, absorbing light. The difference in the final *G*′ values suggests that the presence of cells decreases the elasticity of the films. Previous studies with bovine chondrocyte cells reported interactions with matrix monomers, restricting their polymerisation, and the quenching of free radicals formed from the photoinitiator. These properties can lead to weaker crosslinking in the vicinity of the cells and result in

softer gels,[37] which explains the decreased elasticity of the 3D-printed films with entrapped photosynthetic cells.

At the end of the curing process, G' is an order of magnitude larger than G'', indicating that the ink composed of Alg + GGMMA + LAP is suitable for creating films with solid-like behaviour without the use of $CaCl_2$ or other ionic crosslinkers, which are often used in Alg crosslinking, thus relying solely on photocuring.

Shear stress tolerance of photocured Alg + GGMMA + LAP films was assessed using oscillatory strain sweep measurements with strain amplitudes ranging between 0.1 and 200%. While the overall dynamics of film deformation did not differ significantly with or without cells, there were significant differences in the onset of deformation and the required stress. The films without cells exhibited breakdown at ~6% shear strain, with ~1000 Pa shear stress. This was evident from the sharp decrease in shear stress with increasing shear strain (Fig. 4A black squares). In contrast, films with *Synechocystis* cells showed earlier breakdown, occurring at 5% shear strain with a lower shear stress of ~390 Pa. These films were less durable and more prone to destruction, as indicated by the lower peak in Fig. 4A (yellow dots). Interestingly, films with *Chlamydomonas* cells exhibited higher sheer stress tolerance.

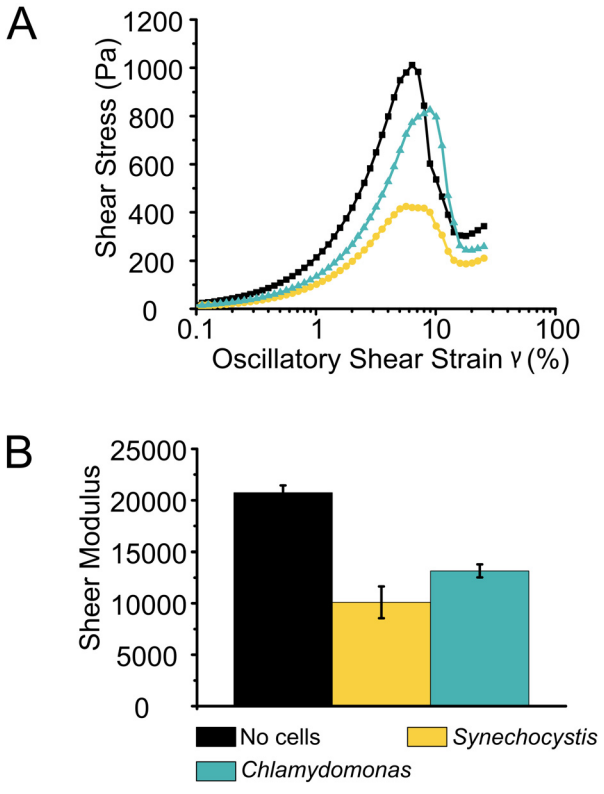

Fig. 4 Rheological properties of photocured films. (A) Oscillatory strain sweeps to measure stress tolerance of 3D-printed films. Oscillatory shear stress is shown in relation to shear strain for inks without cells and with *Synechocystis* and *Chlamydomonas* cells, respectively. Data points represent the average of 2–3 measurements. 20 points per decade were recorded. (B) Average of shear modulus of films without cells, with *Synechocystis* and *Chlamydomonas* cells. The error bars represent the standard deviation of 2–3 measurements.

They started to break down at ~7% strain with 800 Pa shear stress (Fig. 4A cyan triangles). A statistical analysis ($P = 0.0035$ with Kruskal–Wallis test) also confirmed that films with *Chlamydomonas* cells were significantly more shear stress-tolerant compared to those with *Synechocystis* cells.

The rigidity of the films, represented by their shear moduli (Fig. 4B), showed variation among the different samples. The films without cells were significantly more rigid than the other films ($P < 0.006$ with independent sample T-test), followed by films with *Chlamydomonas.* The films with *Synechocystis* cells were the least rigid. However, the rigidity difference between films with *Synechocystis* and *Chlamydomonas* cells was not significant. Interestingly, the presence of cells had a more pronounced impact on the rheological properties of the 3D-printed films compared to Ca^{2+} crosslinked Alg (Ca^{2+}–Alg) or Ca^{2+} and PVA crosslinked, dried TCNF (Ca^{2+}–PVA–TCNF) matrices.[17] It was noted that the presence of the cells affected different matrices to varying degrees. Alg films crosslinked solely with Ca^{2+} ions were more affected, possibly due to interactions between the cells and the Ca^{2+}, which weakens the ionic crosslinking, in contrast to the stronger hydrogen bonds resulting from the drying of nanocellulose films.

By using an Alg + GGMMA + LAP ink formulation and the process of photocuring, robust and durable films were fabricated successfully. These films exhibited elevated levels of elasticity and shear stress tolerance (G' ~ 10–20 kPa, maximum shear stress 390–1000 Pa), significantly outperforming other matrices reported for immobilization, such as Ca^{2+}–Alg hydrogel and dried Ca^{2+}–PVA–TCNF films (G' ~ 1–2 kPa, maximum shear stress 40–75 Pa)[17] or photocurable composites of TCNF and gelatine-methacrylate and GGMMA (30–300 Pa shear stress depending on composition).[38]

These distinctive characteristics position Alg + GGMMA + LAP matrices as a highly suitable scaffolds for hosting photosynthetic microbes, particularly for direct solar chemical production applications. These films have the potential to thrive even in relatively harsh conditions that might involve vigorous agitation or exposure to high ionic strength media.

Coupling the bioink with additive manufacturing enables the creation of structures with tuneable size and shape at a resolution down to micrometre level. These 3D-prints can be utilized in bioreactors with various physical characteristics.

2.3. Biocatalytic production systems in engineered living materials

To validate the applicability of 3D-printed and photocured Alg + GGMMA + LAP biofilms in solar chemical production, we employed two distinct production systems.

Whole-cell biotransformation by green alga. The suitability of 3D-printing using a bioink composed of Alg + GGMMA + LAP as a scaffold was also verified for whole-cell biotransformation using the eukaryotic alga *Chlamydomonas*. This engineered strain is capable of biotransformation of cyclohexanone to ε-caprolactone *via* a heterologously expressed cyclohexanone monooxygenase (CHMO) from *Acinetobacter* NCIB 9871.[30] In this reaction, the substrate is exogenously provided to the

cells. Consequently, it is anticipated that the substrate diffuses into cells, while the product is secreted out into the medium.

With the 3D-printed films, the biotransformation process reached completion in 30 h, effectively converting the majority of the substrate into the product (Fig. 5A). The ratio of the product, ε-caprolactone to the side-product, cyclohexanol was found to be 87% to 13%, respectively. The maximum production rate of ε-caprolactone was 158 ± 2 μmol h^{-1}, while the side-product displayed a formation rate of 28.1 ± 4.8 μmol h^{-1} (Fig. 5B). To assess the specific activity of the cells, the product formation rate was normalised to the total (a + b) Chl content and cell dry weight (DCW). The maximum specific activity reached 0.051 ± 0.003 U mg_{Chl}^{-1} and 3.46 ± 0.2 U g_{DCW}^{-1} (Fig. 5B).

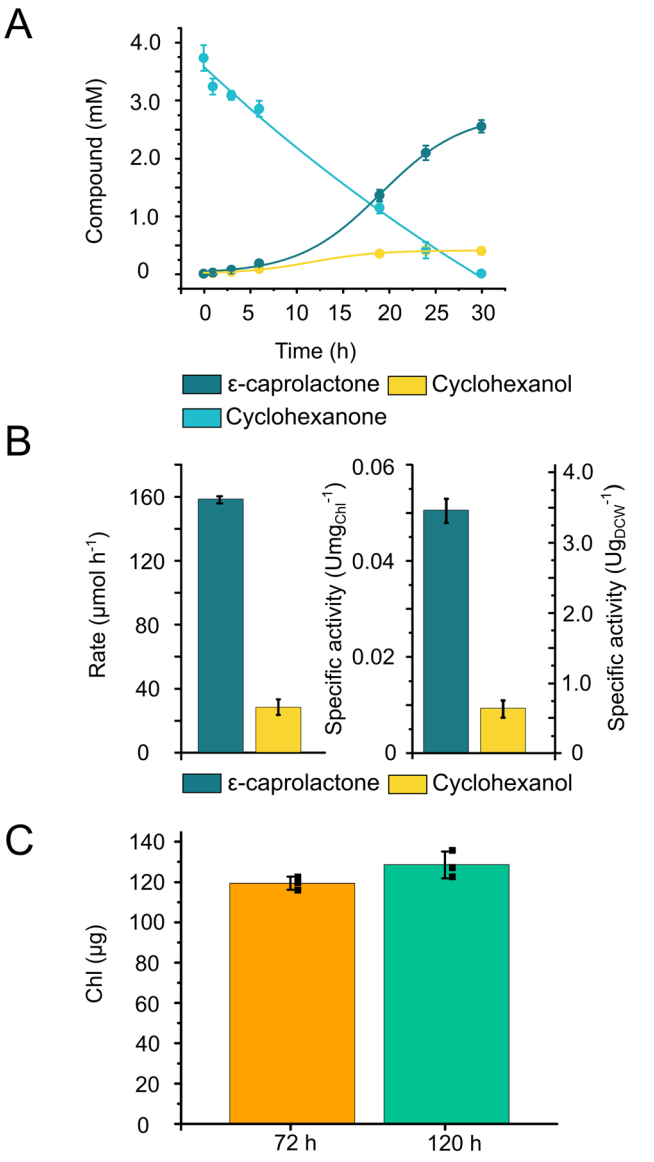

Fig. 5 Whole-cell biotransformation by *Chlamydomonas* cells entrapped in 3D-printed photocured Alg + GGMMA + LAP films. (A) Time course of the formation of ε-caprolactone and cyclohexanol from cyclohexanone. (B) Maximum formation rate of ε-caprolactone and cyclohexanol and specific activity normalised to Chl and DCW of ε-caprolactone and cyclohexanol. (C) Chl content in the films after recovery (72 h after immobilisation and 0 h for biotransformation) and in the end of experiment (120 h after immobilisation).

The entrapped cells produced ε-caprolactone within the printed matrix with a comparable specific activity (3.46 ± 0.2 U g_{DCW}^{-1}) to the biotransformation conducted in suspension cultures (3.6 ± 0.8 U g_{DCW}^{-1}),[30] while the product distribution remained consistent, with 87% of the product formed. During the biotransformation, only a slight increase in the Chl content was detected (Fig. 5C).

Based on these results, we can conclude that the entrapment within the printed matrix neither hinders nor enhances the CHMO-catalysed biotransformation reaction by *Chlamydomonas*. However, this entrapment facilitates the separation of the product and the cells, which is important for potential upscaling endeavours.

Ethylene production by cyanobacteria. Thin films produced through photocuring of the bioink, comprising ethylene-producing *Synechocystis* cells and Alg + GGMMA + LAP, were submerged in the BG11 medium supplemented with 200 mM sodium bicarbonate and 1 mM IPTG in gas-tight vials and illuminated with 35 or 70 μmol photons m^{-2} s^{-1}. IPTG was introduced for the induction of the expression of Efe enzyme in cyanobacterial cells, which is responsible for ethylene biosynthesis.[27] The cyanobacterial films with induced Efe expression demonstrated a gradual increase in ethylene yield until the sixth day, at which point the production virtually ceased under both light conditions (Fig. 6A). A slightly higher ethylene yield was observed under 35 μmol photons m^{-2} s^{-1}, however, the difference is not significant (P > 0.7 with independent sample T-test). The maximum specific ethylene yields reached 780 μmol mg_{Chl}^{-1} under 35 μmol photons m^{-2} s^{-1} illumination and 700 μmol mg_{Chl}^{-1} under 70 μmol photons m^{-2} s^{-1} after seven days. The maximum specific ethylene formation rates were 7.3 and 7.0 μmol mg_{Chl}^{-1} h^{-1}, respectively. Since the two tested light intensities (35 and 70 μmol photons m^{-2} s^{-1}) resulted in comparable ethylene production yields, the data suggests that light saturation already occurs at 35 μmol photons m^{-2} s^{-1} under the studied conditions. For comparison, *Synechocystis* cells entrapped in Ca^{2+}–Alg or Ca^{2+}–PVA–TCNF films were reported to produce between 180 and 400 μmol mg_{Chl}^{-1} ethylene under 35 μmol photons m^{-2} s^{-1} light,[17,39] which is noticeably lower than in our setup. The latter indicates a better biocatalytic performance of photocurable films under submerged cultivation. It is important to note here that these specific production yields could not be directly compared with data obtained by Vajravel and co-authors,[16] where release of ethylene from hydrogel Ca^{2+}–Alg films was simplified by semi-wet cultivation, thus giving higher production yields. The achieved areal yields in photocurable films were 3.7 and 3.5 mmol ethylene m^{-2} under 35 and 70 μmol photons m^{-2} s^{-1}, respectively (Fig. 6A), while the space–time yields were 3.35 mol m_{bicat}^{-3} d^{-1} and 3.30 mol m_{biocat}^{-3} d^{-1}, respectively.

The enhanced ethylene production yield by Alg + GGMMA + LAP films can be attributed to the restricted biomass growth

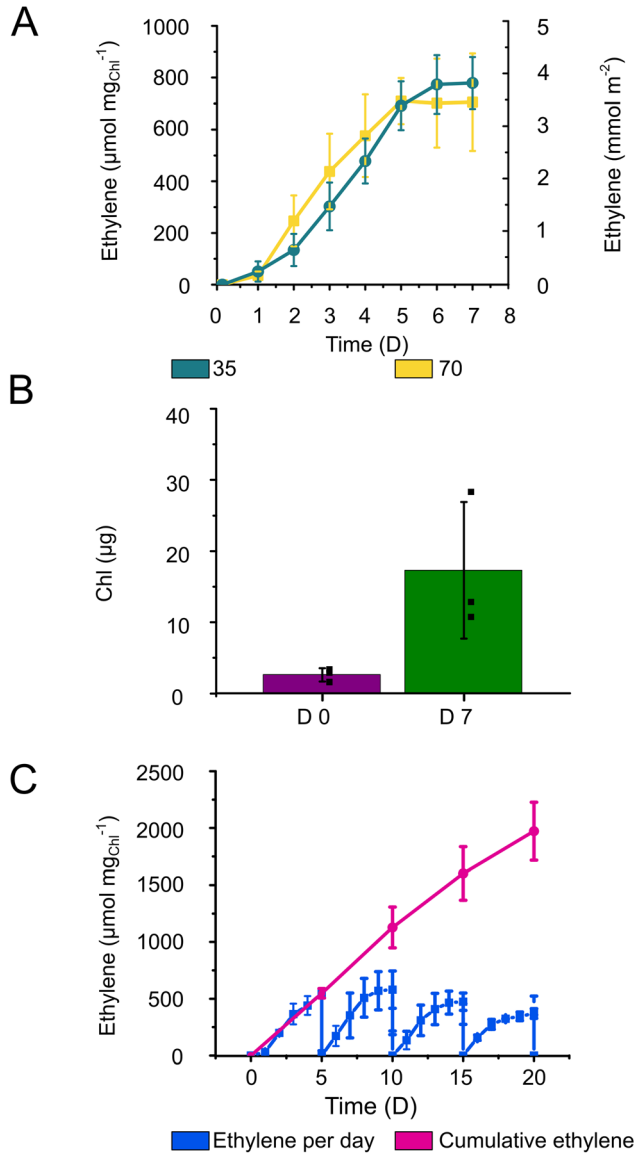

Fig. 6 Ethylene production by *Synechocystis* cells immobilised within 3D-printed photocured Alg + GGMMA + LAP films. (A) The specific and areal ethylene production yields in a batch production system under 35 (teal) or 70 (yellow) µmol photons m^{-2} s^{-1} illumination. (B) Chl contents after overnight recovery (D 0) and 7 days of ethylene production (D 7). (C) Long-term semi-continuous ethylene production and cumulative total ethylene yield during 20-day semi-continuous production. Every 5 days the medium and the headspace were refreshed. The drop of the ethylene concentration to 0 in the end of each cycle is caused by the opening of the vials. Error bars represent the standard deviation of 3 biological (with 2–3 technical) replicates.

and, therefore, better energy and carbon distribution towards the final product. Indeed, the Alg + GGMMA + LAP matrix demonstrated a higher rigidity compared to Ca^{2+}–Alg and Ca^{2+}–PVA–TCNF. High rigidity is known to impede growth of entrapped cells.[40] However, *Synechocystis* within Alg + GGMMA + LAP films still exhibited considerable growth as measured by Chl accumulation (Fig. 6B), which was comparable to one observed in Ca^{2+}–Alg, Ca^{2+}–PVA–TCNF and Ca^{2+}–MLG–TCNF films.[16,17,39] These results highlight the positive effect of the photo-crosslinked Alg + GGMMA + LAP matrix on the ethylene productivity of *Synechocystis* cells.

To assess the potential of 3D-printed Alg + GGMMA + LAP films for long-term applications, ethylene production was monitored for over 20 days using semi-continuous cultivation approach. For this purpose, vials with the films were opened, and the media refreshed every 5th day to ensure an adequate supply of bicarbonate and nutrients to the cells. As a result, ethylene production was extended for up to four cycles. Notably, the highest ethylene yield was obtained in the second cycle, showing a declining trend with subsequent cycles. However, even after the 20th day (4th cycle) the production of ethylene exceeded 350 µmol mg_{Chl}^{-1} (Fig. 6C). Cumulatively, the ethylene yield reached ~2000 µmol mg_{Chl}^{-1} during the 20 days of semi-continuous production (Fig. 6C). In comparison, Vajravel *et al.*[16] reached ~258 µmol ethylene mg_{Chl}^{-1} during the same timeframe.

To sustain ethylene production over an extended duration, periodic medium refreshment is essential to maintain a sufficient supply of nutrients and carbon sources to the cells. However, even with this strategy, it became evident that the ethylene production activity starts gradually declining already at the second cycle of semi-continuous cultivation. A similar inhibitory effect was observed by Vajravel *et al.*[16] in Ca^{2+}–Alg entrapped cells. The decrease in ethylene yield could be potentially linked to the altered C/N metabolism. Furthermore, the increased cell density within the films might impose limitations, leading to the inactivation of cell metabolism or cell death.[16]

Unlike Ca^{2+}–Alg films, the photocured Alg + GGMMA + LAP films did not disintegrate in the medium supplemented with 200 mM sodium bicarbonate, indicating sufficient performance in environments with increased ionic strength.[17] It is worth mentioning though, that during the long-term semi-continuous production a few films became detached from the glass surface, subsequently fracturing due to agitation. Despite fracturing, the ethylene production activity was not affected.

In summary, the experiments demonstrated successful application of the photocurable matrix composed of Alg, GGMMA and the photoinitiator LAP for immobilisation of engineered *Synechocystis* cells within thin films using 3D-printing technology with photocuring. These films showed sufficient stability and sustained biocatalytic activity for over an extended timeframe with the highest reported ethylene yield from the utilised strain in comparable production systems.

3. Conclusion

We conducted a comprehensive evaluation of the Alg + GGMMA + LAP photocurable bioink for 3D-printing of photosynthetic biocatalysts, specifically for the entrapment of the ethylene-producing cyanobacterium *Synechocystis* and eukaryotic green alga *Chlamydomonas* capable of converting cyclohexanone to ε-caprolactone. The rheological measurements indicated the formation of rigid and mechanically stable films

from the bioink under 405 nm illumination without applying any ionic crosslinkers.

Although a temporary reduction in the photochemical activity of the entrapped cells was initially observed following printing, the rapid and substantial subsequent recovery underscores the remarkable biocompatibility of the ink, thus confirming its minimal adverse impact on both photosynthetic microorganisms. The engineered living material exhibited notable efficacy in both the production of photosynthetic ethylene and the biotransformation of cyclohexanone to ε-caprolactone, both of which hold considerable commercial significance. Furthermore, the Alg + GGMMA + LAP bioink, when coupled with ethylene-producing *Synechocystis*, achieved the highest reported specific ethylene production yield among polymer hydrogel matrices. The latter validated and reinforced the idea that advanced materials together with optimised conditions could significantly enhance chemical production of solid-state cell factories.

The photocurable matrix, made of the wood-derived biopolymer GGMMA and seaweed-derived Alg, is a robust environmentally friendly material that is compatible with photosynthetic microorganisms. These qualities unlock numerous potential applications, including the production of various chemicals, wastewater treatment, and atmospheric CO_2 removal. When integrated with 3D-printing technologies, the Alg + GGMMA + LAP photocurable composite enables the efficient fabrication of complex hierarchical structures. As we continue to explore their applications and harness their potential in combination with various microorganisms, Alg + GGMMA + LAP photocurable composites present an opportunity for advancing towards a more sustainable and environmentally friendly chemical industry.

4. Experimental

4.1. Strains and culture conditions

Synechocystis PCC 6803 *efe* strain expressing ethylene forming enzyme (Efe)[27] was used for ethylene production and *Chlamydomonas reinhardtii* UVM11-CW/CHMO_PSAD clone 10 (*Chlamydomonas*)[30] was used for the biotransformation of cyclohexanone to ε-caprolactone.

Stock cultures of *Synechocystis* were kept in 25 mL BG11 medium[41] containing 10 μg mL^{-1} chloramphenicol and 25 μg mL^{-1} spectinomycin under 1% CO_2 at 30 °C with 100 rpm orbital shaking and under 50 μmol photons m^{-2} s^{-1} illumination measured by Li-250A light meter (Li-cor Biosciences, USA). Stock cultures of *Chlamydomonas* were kept in Tris-acetate-phosphate (TAP) medium[42] containing 100 μg mL^{-1} spectinomycin at 25 °C with 120 rpm orbital shaking under 35 μmol photons m^{-2} s^{-1} illumination. Experimental cultures of *Synechocystis* were grown in 100 mL BG11 medium with 100 rpm orbital shaking under 70 μmol photons m^{-2} s^{-1} illumination and *Chlamydomonas* cultures were grown in 200 mL TAP medium with 120 rpm orbital shaking under 35 μmol photons m^{-2} s^{-1} illumination.

4.2. Galactoglucomannan-methacrylate (GGMMA) synthesis

GGMMA was synthesised according to Xu *et al.* (2019).[25] 1 g of galactoglucomannan (GGM) was dissolved in 100 mL deionized water overnight at 50 °C. After dissolution, 2 mL methacrylate anhydride was added and the reaction proceeded for 3 h at pH 8.0, controlled by the addition of 5 M NaOH. GGMMA was purified by dialysis to remove unreacted methacrylate anhydride (cut-off of 2 kDa). The purified samples were lyophilized and stored protected from light. GGMMA was characterized by NMR and chromatographic HPSEC. The resulting degree of substitution was 1.61 mmol g^{-1} and the average molecular weight was 2.619×10^4 g mol^{-1}.

4.3. Ink formulation and 3D-printing

The ink for 3D-printing was prepared by dissolving alginate (Alg), GGMMA and lithium phenyl-2,4,6-trimethylbenzoylphosphinate (LAP) in water and adding concentrated *Synechocystis* cells with a chlorophyll (Chl) concentration of ~10 μg Chl *a* mL^{-1} ink or *Chlamydomonas* cells with ~100 μg Chl (*a* + *b*) mL^{-1} ink. The components were mixed well using a pipette tip and vortex. The final concentration of the dry materials was 3% (w/v) Alg, 4% (w/v) GGMMA and 0.05% (w/v) LAP. The ink was loaded into a syringe with a piston (Nordson, USA), and the print was made using a 25G needle nozzle (Nordson, USA) with Brinter ONE multitool 3D bioprinter (Brinter, Finland) on 6 cm × 2 cm glass slides for *Synechocystis* and 4 cm × 1 cm for *Chlamydomonas*. The areas of the prints were 11.21 cm^2 and 3 cm^2, respectively. The glass slides were pre-treated with 3-(trimethoxysilyl)propyl methacrylate (TMPSM) to help the attachment of the 3D-printed biofilms to their surface. The methacrylate groups in GGMMA form covalent bonds with the methacrylate on the treated glass surface. The films were photocured by exposing them to 60 mW cm^{-2} intensity light with a wavelength of 405 nm for 10 min. After photocuring, the slides were placed on a Petri dish in BG11 medium to recover overnight. After recovery they were transferred to infusion bottles in 10 mL BG11 medium supplemented with 200 mM sodium bicarbonate (*Synechocystis*) or 5 mL TAP (*Chlamydomonas*). The bottles were sealed with a rubber septum.

4.4. Glass treatment

The glass surface was cleaned with ethanol, then soaked in 5% (v/v) HCl for 4 h to remove any remaining surface contaminants. The slides were then rinsed and submerged in reverse osmosis water overnight. The next day the slides were dried and submerged in a 2% (w/v) TMPSM (Sigma-Aldrich, US) solution in 95% (v/v) ethanol pH 4.5–5.5 (adjusted with acetic acid). They were gently agitated in the solution for 2 min followed by rinsing with 99% (v/v) ethanol and drying.

4.5. Rheology measurements

Rheology measurements were performed at room temperature with a MCR 702 MultiDrive rheometer (Anton Paar GmbH, Germany) with a PP25 parallel-plate (diameter: 25 mm, gap:

0.2 mm). Photo-rheology measurements were performed with constant strain of 0.5% and frequency of 5 Hz. A sample of 982 μL was irradiated with 60 mW cm^{-2}, 405 nm light (bluepoint 4 ecocure UV lamp, The Hönle Group, Germany) 20 s after the strain was applied. Amplitude sweep was performed to investigate the stress tolerance of the films with an amplitude of 0.01–200% and frequency of 5 Hz. 20 points per decade were recorded. The films were first cured for 10 min on the glass plate of the rheometer as described above.

Storage modulus (G') describing elasticity, loss modulus (G'') describing viscosity and loss factor tangent ($\tan\delta$) the ratio of storage and loss moduli (G''/G') were recorded.

4.6. Photosynthetic activity measurements

PAM 2000 Portable Chlorophyll Fluorometer (Walz, Germany) was used to determine PSII yield. Measurements were taken right after 3D-printing and every day for 6 days afterwards. For the measurement, glass slides with a printed film were placed under the sensor. The samples were subjected to saturating light pulses with 3000 μmol m^{-2} s^{-1} light intensity for 0.8 s applied on top of 70 μmol m^{-2} s^{-1} actinic light for 315 s to probe the effective yield of photosystem II (Y(II)).

4.7. Ethylene production and determination

After printing, the films were left to recover overnight in Petri dishes in BG11 medium under 25 μmol photons m^{-2} s^{-1} illumination. After recovery, the films were placed in the gas-tight, 126 mL vials containing 10 mL BG11 medium supplemented with 200 mM sodium bicarbonate and 1 mM IPTG. The vials were incubated at 30 °C with 60 rpm orbital shaking and under 35 or 70 μmol photons m^{-2} s^{-1}. For the short-term ethylene production, samples were taken from the headspace of the vials every day using a gastight syringe (Hamilton, US). To determine the ethylene concentration, a 40 μL sample was injected manually in Clarus 580 gas chromatograph (GC) (PerkinElmer, USA). The GC was equipped with the Carboxen 1010 PLOT 30 m × 0.53 mm capillary column operating at 140 °C and a flame ionisation detector (FID) operating at 350 °C. The airflow and H_2 flow were 300 mL min^{-1} and 30 mL min^{-1} respectively. Argon was used as carrier gas with a flow rate of 9.8 mL min^{-1}. Ethylene concentration in the liquid phase and headspace was calculated based on the partial pressure and solubility of ethylene at 30 °C.

For the long-term (20-day) experiment, the vials were opened every 5 days and the medium was replaced with fresh one containing bicarbonate and IPTG. Samples for ethylene measurements were taken every day and analysed as described above. Ethylene yield was normalised to the initial Chl content.

4.8. Biotransformation of cyclohexanone to ε-caprolactone using *Chlamydomonas*

After printing, the films were left to recover in TAP for three days under 20 μmol photons m^{-2} s^{-1} illumination at 25 °C, and ambient air. Biotransformation by *Chlamydomonas* cells was performed in 37 mL infusion bottles with a gas-tight rubber stopper starting with 3.25 mL biotransformation mix (5 mM cyclohexanone, 1.7% (v/v) ethanol, 25 mM MOPS pH 7.2 in TAP medium).[30] The films were agitated by orbital shaking with 90 rpm under 26 μmol photons m^{-2} s^{-1} illumination. 250 μL samples were taken at different time points during the biotransformation (0, 1, 3, 6, 19, 24, 30, 43, 48, 72 h) and stored at −80 °C. For sample extractions, 0.06% (v/v) HCl was added. Extraction with ethyl acetate containing 2 mM acetophenone as internal standard was done twice by addition of ethyl acetate to half the volume of the sample, vigorous mixing, centrifugation with 21 130*g* for 1 min, collecting the upper phase separately, and repeating the steps once more. The ethylene phase was dried using anhydrous $MgSO_4$ (Sigma Aldrich, USA). After vigorous mixing and centrifugation at 21 130*g* for 4 min, the supernatants were used for gas chromatography analysis.

Samples were analysed with a GC2010 Pro GC (Shimadzu, Japan) equipped with a FID, AOC-20s autosampler, AOC-20i autoinjector, and a HP-5MS 30 m × 0.25 mm (5%-phenyl)-methylpolysiloxane column (19091S-133, Agilent). Nitrogen was used as the carrier gas.

Calibration of the GC was performed using various concentrations of cyclohexanone, cyclohexanol, acetophenone, and ε-caprolactone using cyclopentanone as an internal standard with 2 mM concentration (Sigma Aldrich, US). Concentrations of the compounds in the samples were calculated with response factors from the calibration.

Specific activity was calculated based on the formation of the compound as units, where a unit represents μmol min^{-1}. Rates were normalised to the initial chlorophyll content of the film or to dry cell weight. The formation followed a sigmoidal curve, and the maximal reaction velocity was calculated with Origin 2016 (64-bit) Sr2 b9.3.3.303 (OriginLab Corporation) using slogistics2 fitting.

4.9. Chlorophyll extraction and determination

After 3D-printing and photocuring, a film was removed from the glass slide using a spatula and placed into an Eppendorf tube. For *Synechocystis* containing films 1 mL 90% (v/v) methanol was added, and the film was incubated at 60 °C for 1 h in darkness. The samples were centrifuged, and Chl *a* concentration was determined by measuring absorbance of the supernatant at 665 nm using UV-1800 spectrophotometer (Shimadzu, Japan). Chl *a* concentration was calculated according to Lichtenthaler.[43]

For *Chlamydomonas*, the chlorophyll from 3D-printed films was extracted with 5 mL methanol (Sigma Aldrich, France) by incubating 20 min at +60 °C. Absorbance from the supernatant was measured with UV-1800 spectrophotometer at 652, 665.2, and 750 nm. The total chlorophyll content (Chl *a* + *b*) was calculated according to Porra *et al.*[44]

Author contributions

Conceptualisation YA, CX; methodology YA, CX, WX, OB, SK, VS, GST; formal analysis GST, TS; investigation GST, OB, TS;

resources YA, CX; writing – original draft GST; writing – review & editing all authors.

Conflicts of interest

There are no conflicts to declare.

Acknowledgements

This work was supported by the Novo Nordisk Foundation project "PhotoCat" (project no. NNF20OC0064371 to YA), the NordForsk Nordic Center of Excellence "NordAqua" (no. 82845 to YA), the EU FET Open project "FuturoLEAF" (grant agreement no. 899576 to YA), the Academy of Finland "Photo-e-Mat" (project no. 353140 to YA and 356645 to CX) and "AI-4-LCC" (project no. 341596 to CX) projects.

References

1 C. Tan, P. Xu and F. Tao, *Trends Biotechnol.*, 2022, **40**, 1488–1502.
2 J. Wichmann, K. J. Lauersen, N. Biondi, M. Christensen, T. Guerra, K. Hellgardt, S. Kühner, M. Kuronen, P. Lindberg, C. Rösch, I. S. Yunus, P. Jones, P. Lindblad and O. Kruse, *Trends Biotechnol.*, 2021, **39**, 323–327.
3 X. Xu, T. Hilberath and F. Hollmann, *Curr. Opin. Green Sustain. Chem.*, 2023, **39**, 100745.
4 A. Dawiec-Liśniewska, D. Podstawczyk, A. Bastrzyk, K. Czuba, K. Pacyna-Iwanicka, O. V. Okoro and A. Shavandi, *Biotechnol. Adv.*, 2022, **59**, 107988.
5 G. S. Caldwell, P. In-na, R. Hart, E. Sharp, A. Stefanova, M. Pickersgill, M. Walker, M. Unthank, J. Perry and J. G. M. Lee, *Energies*, 2021, **14**, 2566.
6 S. Kosourov, G. Murukesan, M. Seibert and Y. Allahverdiyeva, *Algal Res.*, 2017, **28**, 253–263.
7 S. N. Kosourov, M. He, Y. Allahverdiyeva and M. Seibert, Immobilization of Microalgae as a Tool for Efficient Light Utilization in H_2 Production and Other Biotechnology Applications, in *Microalgal Hydrogen Production: Achievements and Perspectives*, ed. M. Seibert and G. Torzillo, The Royal Society of Chemisty (RSC), London, UK, 2018, ch. 15, pp. 355–384.
8 S. Vasilieva, E. Lobakova and A. Solovchenko, in *Environmental Biotechnology Vol. 3*, ed. K. M. Gothandam, S. Ranjan, N. Dasgupta and E. Lichtfouse, Springer International Publishing, Cham, 2021, pp. 193–220.
9 A. Léonard, P. Dandoy, E. Danloy, G. Leroux, C. F. Meunier, J. C. Rooke and B.-L. Su, *Chem. Soc. Rev.*, 2011, **40**, 860–885.
10 M. Jämsä, S. Kosourov, V. Rissanen, M. Hakalahti, J. Pere, J. A. Ketoja, T. Tammelin and Y. Allahverdiyeva, *J. Mater. Chem. A*, 2018, **6**, 5825–5835.
11 H. Leino, S. N. Kosourov, L. Saari, K. Sivonen, A. A. Tsygankov, E.-M. Aro and Y. Allahverdiyeva, *Int. J. Hydrogen Energy*, 2012, **37**, 151–161.
12 J. Aggarwal, S. Sharma, H. Kamyab and A. Kumar, *J. Environ. Treat. Tech.*, 2020, **8**, 1005–1016.
13 L. Liu and S. Choi, in 2019 IEEE 32nd International Conference on Micro Electro Mechanical Systems (MEMS), 2019, pp. 222–225.
14 N. Mallick and L. C. Rai, *World J. Microbiol. Biotechnol.*, 1994, **10**, 439–443.
15 P. Sikareepaisan, U. Ruktanonchai and P. Supaphol, *Carbohydr. Polym.*, 2011, **83**, 1457–1469.
16 S. Vajravel, S. Sirin, S. Kosourov and Y. Allahverdiyeva, *Green Chem.*, 2020, **22**, 6404–6414.
17 V. Rissanen, S. Vajravel, S. Kosourov, S. Arola, E. Kontturi, Y. Allahverdiyeva and T. Tammelin, *Green Chem.*, 2021, **23**, 3715–3724.
18 V. Guccini, J. Phiri, J. Trifol, V. Rissanen, S. M. Mousavi, J. Vapaavuori, T. Tammelin, T. Maloney and E. Kontturi, *ACS Appl. Polym. Mater.*, 2022, **4**, 24–28.
19 C. G. Williams, A. N. Malik, T. K. Kim, P. N. Manson and J. H. Elisseeff, *Biomaterials*, 2005, **26**, 1211–1218.
20 S. Kumar, K. Habib and T. Fatma, *Sci. Total Environ.*, 2008, **403**, 130–138.
21 S. S. Stalling, S. O. Akintoye and S. B. Nicoll, *Acta Biomater.*, 2009, **5**, 1911–1918.
22 I. Chiulan, E. B. Heggset, Ș. I. Voicu and G. Chinga-Carrasco, *Biomacromolecules*, 2021, **22**, 1795–1814.
23 Y.-R. Lou, L. Kanninen, T. Kuisma, J. Niklander, L. A. Noon, D. Burks, A. Urtti and M. Yliperttula, *Stem Cells Dev.*, 2014, **23**, 380–392.
24 K. Markstedt, A. Mantas, I. Tournier, H. Martínez Ávila, D. Hägg and P. Gatenholm, *Biomacromolecules*, 2015, **16**, 1489–1496.
25 W. Xu, X. Zhang, P. Yang, O. Långvik, X. Wang, Y. Zhang, F. Cheng, M. Österberg, S. Willför and C. Xu, *ACS Appl. Mater. Interfaces*, 2019, **11**, 12389–12400.
26 H. Lee, D. Shin, J. Choi, C. S. Ki and J. Hyun, *Carbohydr. Polym.*, 2022, **290**, 119485.
27 K. Thiel, E. Mulaku, H. Dandapani, C. Nagy, E.-M. Aro and P. Kallio, *Microb. Cell Fact.*, 2018, **17**, 34.
28 V. P. Haribal, Y. Chen, L. Neal and F. Li, *Engineering*, 2018, **4**, 714–721.
29 J. Ungerer, L. Tao, M. Davis, M. Ghirardi, P.-C. Maness and J. Yu, *Energy Environ. Sci.*, 2012, **5**, 8998–9006.
30 V. Siitonen, A. Probst, G. Tóth, R. Kourist, M. Schroda, S. Kosourov and Y. Allahverdiyeva, *Green Chem.*, 2023, **25**, 5945–5955.
31 S. Kodru, A. ur Rehman and I. Vass, *Photosynth. Res.*, 2020, **145**, 227–235.
32 A. Latifi, M. Ruiz and C.-C. Zhang, *FEMS Microbiol. Rev.*, 2009, **33**, 258–278.
33 N. Häubner, R. Schumann and U. Karsten, *Microb. Ecol.*, 2006, **51**, 285–293.
34 M. Leupold, S. Hindersin, G. Gust, M. Kerner and D. Hanelt, *J. Appl. Phycol.*, 2013, **25**, 485–495.

35 S. M. Hull, L. G. Brunel and S. C. Heilshorn, *Adv. Mater.*, 2022, **34**, 2103691.
36 L. Yuan, Y. Wu, Q. Gu, H. El-Hamshary, M. El-Newehy and X. Mo, *Int. J. Biol. Macromol.*, 2017, **96**, 569–577.
37 S. Chu, M. M. Maples and S. J. Bryant, *Acta Biomater.*, 2020, **109**, 37–50.
38 Q. Wang, O. Backman, M. Nuopponen, C. Xu and X. Wang, *Front. Chem. Eng.* , 2021, **3**, 723429.
39 T. Virkkala, S. Kosourov, V. Rissanen, V. Siitonen, S. Arola, Y. Allahverdiyeva and T. Tammelin, *J. Mater. Chem. B*, 2023, **11**, 8788–8803.
40 D. J. Dickson, C. J. Page and R. L. Ely, *Int. J. Hydrogen Energy*, 2009, **34**, 204–215.
41 R. Rippka, J. Deruelles, J. B. Waterbury, M. Herdman and R. Y. Stanier, *Microbiology*, 1979, **111**, 1–61.
42 E. H. Harris, *The Chlamydomonas Sourcebook: Introduction to Chlamydomonas and Its Laboratory Use: Volume 1*, Academic Press, 2009.
43 H. K. Lichtenthaler, *Methods in Enzymology*, Academic Press, 1987, vol. 148, pp. 350–382.
44 H. Scheer, R. J. Porra and J. M. Anderson, *Photochem. Photobiol.*, 1989, **50**, 403–412.

